RSC Advances

PAPER

View Article Online
View Journal | View Issue

Check for updates

Cite this: *RSC Adv.*, 2025, **15**, 44194

Theoretical determination of electronic properties of resorcinol and hydroquinone as building blocks of molecular wires

Jhon S. Martínez,[a] Daniel Gallego *[a] and Judith H. Ojeda S. *[b]

This study presents a theoretical and computational analysis of resorcinol and hydroquinone as potential molecular wire components, employing the tight-binding Hamiltonian formalism within a real-space decimation approach based on Green's functions. We investigated their electronic transport properties, specifically electrical current and conductance, by varying key parameters such as the atomic site energy, the coupling energy, and the electrode attachment configurations. We found a semiconductor behavior in both molecules, reaching their maximum electron capacity at around 5 V. In addition, we analyzed the substituent patterns of hydroxyl groups on the aromatic ring by comparing the results of both molecules. Our findings highlight the critical influence of the aromatic ring's inner coupling energy and the hydroxyl groups' atomic site energy on electronic transport. The strong inner coupling regime in the aromatic ring demonstrated better transmission probability in accordance with the aromatic sp^2 hybridization moiety. Due to the disubstitution pattern in resorcinol, the coupling between the hydroxyl groups and the aromatic ring plays a crucial role in electron conductance in this system, as demonstrated by the diminishing the polarization of electrons from the hydroxyl to the aromatic ring by the weakening of the energy coupling. Notably, we observed a stark contrast between the two molecules: resorcinol, characterized by *meta*-disubstitution, exhibits quantum interference effects, while hydroquinone, with *para*-disubstitution, facilitates a more stable and efficient electronic flux. Interestingly, comparing our results with those of previously reported aromatic conductors, such as benzene and catechol, we found that for both systems (*i.e.*, resorcinol, hydroquinone), the voltage threshold is lower, with hydroquinone a particularly promising system, reaching $I/I_0 = 0.45$ at V = 1.2 V, almost doubling the values of all the other compared systems. These results showcase resorcinol and hydroquinone as promising candidates for molecular wire applications in electronic devices.

Received 15th August 2025
Accepted 18th October 2025

DOI: 10.1039/d5ra06041a

rsc.li/rsc-advances

Open Access Article. Published on 12 November 2025. Downloaded on 5/4/2026 11:46:22 PM.
This article is licensed under a Creative Commons Attribution-NonCommercial 3.0 Unported Licence.

1 Introduction

During the last few decades, miniaturizing electronic components, such as semiconductors and transistors, has attracted research in materials development to improve energy efficiency, increase processing speed, and decrease environmental impact.[1–3] Advanced applications, such as bio-sensing, artificial intelligence, cloud computing, and quantum computing, require enormous processing power.[2,4,5] Additionally, the large volume of electronic waste from the electronics industry and the physical limits of component miniaturization present significant challenges. Reducing the sizes of transistors and semiconductors enables the construction of more powerful processors capable of handling these workloads, increases the working life of electronic devices, and shrinks the waste volume in their end of life.[6–9]Transistors are silicon-based materials that are the primary components of circuits condensed in small areas, which frequently experience overheating, leading to a decrease in their resistance. These issues are not limited to transistors; they also impact semiconductors whose particle size alters their physical properties. Thus, some problems arise, including fluctuations in concentration, dopant surface diffusion, alterations in charge transfer mechanisms, stress, limitations on the maximum current per unit volume of conductive material, heat dissipation, and decreased reliability.[9–11] Scientists have sought novel materials and structures to overcome the challenges in semiconductor research and optimize performance in practical applications. Among those, molecular electronics is one of the alternatives due to the nanoscale dimensions of individual molecules and the inherent self-assembly properties of molecules for integration into electronic devices. For instance, electronic systems, such as wires, switches, rectifiers, and memories, can be built up by utilizing molecules as nanoscale unit blocks.[12–15] On the other hand,

[a]*Laboratorio de Diseño y Síntesis de Sistemas Químicos (DiSi$_2$Quim), Facultad de Ciencias, Universidad Pedagógica y Tecnológica de Colombia, Tunja, Colombia. E-mail: daniel.gallego@uptc.edu.co; judith.ojeda@uptc.edu.co*

[b]*Grupo de Física de Materiales, Facultad de Ciencias, Universidad Pedagógica y Tecnológica de Colombia, Tunja, Colombia*

© 2025 The Author(s). Published by the Royal Society of Chemistry

Open Access Article. Published on 12 November 2025. Downloaded on 5/4/2026 11:46:22 PM.
This article is licensed under a Creative Commons Attribution-NonCommercial 3.0 Unported Licence.

according to Biswal *et al.*[16] "Usually, the organic molecules with π-conjugated molecular systems and heteroatoms like oxygen, sulphur and nitrogen show off electron transport property. The electron transport property of the molecules is reinforced further, depending on the nature of the substituent available in the molecule." This highlights the significance of specific structural features in the electronic properties of organic molecules, which is crucial for their application in electronic devices.[16] Aromatic molecules possess different functionalities that make them interact intermolecularly and with their surroundings, commonly known as π–π, π-functional groups, π-cation, and functional groups-surroundings.[11,13,15] Thus, we are interested in studying one of the shortest aromatic compounds, composed of an aromatic ring and heteroatom functionalities, to interact with metallic surfaces and understand the electrical properties by evaluating the electron transport along the chemical backbone. Hence, we focus on the isomers of benzenediols, with the condensed chemical formula $C_6H_6O_2$, known as catechol, resorcinol and hydroquinone (Fig. 1), differentiated from each other by the substitution pattern of both hydroxyl groups. Our interest in these molecules relies on the fact that benzenediols are the smallest aromatic building block of natural dyes such as anthocyanins and flavonoids,[17] which are larger π-conjugated systems; thus, understanding the electronic behavior of these small entities allows us to study larger molecules, such as natural dyes, evaluating their potential application as molecular wires.

Prior to this work, we modeled and studied catechol connected to electrodes in different fashions.[18] In this work, we focus on resorcinol and hydroquinone by attaching the hydroxyl groups to metallic leads because this configuration is the most favorable for interaction with the environment. To analyze the electronic transport properties of both molecules, we employed a tight-binding Hamiltonian formalism combined with a real-space decimation approach using Green's functions.[19–25] This methodology allows us to determine the transmission probability, current, and conductance.[18,26–36] We calculated the transmission probability and the conductance through Green's functions. In contrast, we derived the current using the Landauer–Büttiker formalism, allowing us to establish a quantitative relationship between electron transmission probability and electrical conductance in mesoscopic systems. This framework serves as the foundation for understanding and predicting the electronic behavior of materials and devices on nanometric and micrometric scales, with significant implications for the design and development of advanced electronic technologies.[37–42] Herein, we investigate the electrical properties of resorcinol and hydroquinone, understanding how the transport processes vary by the influence of certain factors such as coupling to the leads, bond interactions, and the electrical injection potential.

2 Method and calculation

2.1 Theoretical model

We define our model as each benzenediol isomer anchored between two electrodes linked through the hydroxyl groups (Fig. 2). We label each atom as an atomic site to define the system's energy and the atomic interaction, represented by the bonds, as coupling energies. Thus, the site energy of the carbon atoms is E_c, while the site energy of the hydroxyl groups is E_{OH} (Fig. 3). Here t_c describes the carbon–carbon bond coupling energy, and w corresponds to the bond coupling energy between the hydroxyl group and the aromatic ring.[3,13,18,29–31,43]

Within the framework of the tight-binding approximation, a general Hamiltonian characterizing these systems is expressed as follows:[13,30–36]

$$H = H_{AR} + H_L + H_I \quad (1)$$

In our case, H_{AR} represents the Hamiltonian associated with the aromatic compounds (*i.e.*, resorcinol and hydroquinone), H_L corresponds to the Hamiltonian of the leads, and H_I is the Hamiltonian of the interaction between the molecule and the leads. The expression for H_{AR} is given as follows:[13,30,31]

$$H_{AR} = \sum_i t_i \left(c_i^\dagger c_{(i+1)} + c_{(i+1)}^\dagger c_i \right) + \sum_i E_i c_i^\dagger c_i, \quad (2)$$

where t_i is the coupling between the atomic sites of the system, E_i represents the energy of the atomic sites and c_i ($c_i^\dagger$) is the creation (destruction) operator of the electron at atomic site i.

Conversely, the Hamiltonians of the leads (H_L) and the interaction between the leads and the molecule (H_I) are expressed as follows:[13,30,31]

$$H_L = \sum_{k_L} \varepsilon_{k_L} d_{k_L}^\dagger d_{k_L} + \sum_{k_R} \varepsilon_{k_R} d_{k_R}^\dagger d_{k_R}, \quad (3)$$

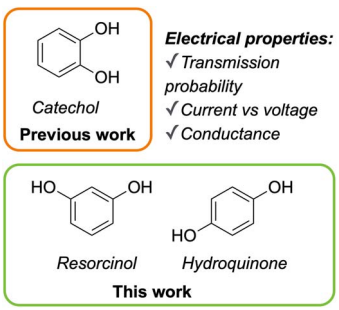

Fig. 1 Structures of the benzenediols isomers and electrical properties evaluated in these molecular systems.

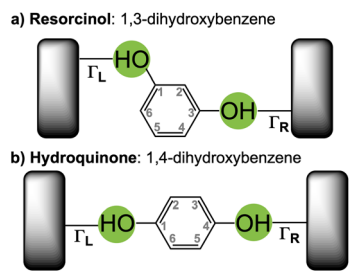

Fig. 2 Molecular models of the (a) resorcinol and (b) hydroquinone anchored between two electrodes. Γ_L and Γ_R refer to the functions of coupling of the molecule to the left and right leads.

Open Access Article. Published on 12 November 2025. Downloaded on 5/4/2026 11:46:22 PM.
This article is licensed under a Creative Commons Attribution-NonCommercial 3.0 Unported Licence.

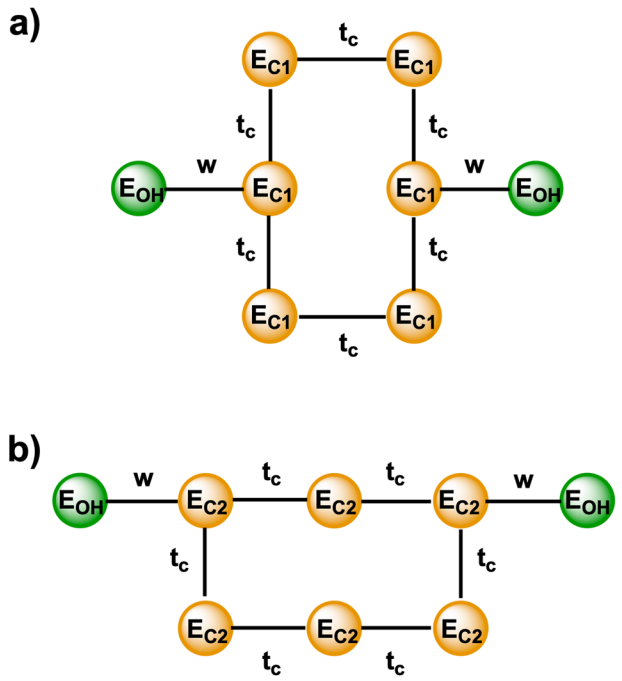

Fig. 3 Geometric models for (a) hydroquinone and (b) resorcinol, with all energy sites and interactions in the system. E_{C1} and E_{C2} are the energy at each carbon for hydroquinone and resorcinol, respectively.

$$H_I = \sum_{k_L} \Gamma_L d^{\dagger}_{k_L} c_1 + \sum_{k_R} \Gamma_R d^{\dagger}_{k_R} c_N + h.c., \tag{4}$$

where $d^{\dagger}_{k_{L(R)}}$ is the creation operator of an electron in a state $k_{L(R)}$ with energy $\varepsilon_{k_{L(R)}}$, $\Gamma_{L(R)}$ is the coupling between each lead with the aromatic molecule, and *h.c.* is the Hamiltonian's complex conjugate. To make the analytical procedure computationally practical, we conduct a decimation procedure for both molecules, which undertakes all energy interactions and transforms the Hamiltonian into an effective linear chain.

It is worth noting that although the molecular systems selected in this study are relatively compact (*i.e.*, resorcinol and hydroquinone), the application of real-space renormalization remains both appropriate and advantageous for analyzing quantum transport. This technique does not involve any physical deformation or literal linearization of the molecular geometry. Instead, it provides a mathematical transformation of the system, governed by a tight-binding Hamiltonian (as mentioned), into an effective one-dimensional chain. This mapping retains the essential physical and electronic properties of the original structure by embedding the molecular topology, site connectivity, and inter-site couplings into the renormalized site energies and hopping integrals.

This formalism has been successfully applied even in small π -conjugated molecules and biomolecular systems. For instance, Zhouyin *et al.* developed a differentiable nonequilibrium Green's function framework[44] that retains quantum transport characteristics through effective parameterizations. Similarly, Marie and Loos employed a similarity renormalization group to derive effective Green's functions for molecular systems,[45] demonstrating the technique's ability to preserve electron correlation and transport-relevant properties. Furthermore, Lyu and Kawashima further confirmed the robustness of three-dimensional real-space renormalization methods with well-controlled approximations, even in reduced systems.[46]

In the specific case of molecular electronics, renormalization offers a physically meaningful and computationally efficient approach to evaluating quantum interference phenomena. Even for small systems, quantum interference is not a size-dependent phenomenon but a consequence of coherent electron propagation through multiple pathways within a conjugated molecular structure. These effects become particularly prominent in systems with different substitution patterns, such as *meta vs. para*-disubstitution, which modify the symmetry and phase coherence of the conducting orbitals.

2.2 Decimation procedure

As mentioned above, we performed decimation to reduce the computational and mathematical complexity of the system. Using the geometric model shown in Fig. 3, we conducted this procedure using Green's functions. Specifically, we employ the Dyson equation:

$$G = G^0 + G^0(\Sigma_L + \Sigma_R)G, \tag{5}$$

where G^0 is the bare Green's function of the isolated molecule, and $\Sigma_{L(R)}$ represents the self-energies of the left and right leads, respectively. This approach, within a real-space renormalization scheme, effectively transforms the two-dimensional geometric model into a one-dimensional framework that integrates all energy interactions.[13,18,29–31,43]

After applying the decimation process, we reordered each molecule into an effective linear chain. Thus, we used the Dyson equation to further simplify the planar structures of resorcinol and hydroquinone, with two degrees of freedom, into a linear system with a single degree of freedom (Fig. 4).Consequently, the transmission probability ($T(E)$) can be determined using the Fisher–Lee relationship, yielding the following expression:[3,13,30,31,47]

$$T(E) = \frac{\Gamma^2 \left(G^0_{1N}\right)^2}{\left|\left[1 + \frac{i}{2}\Gamma G^0_{NN}\right]^2 + \frac{\Gamma^2}{4}\left(G^0_{1N}\right)^2\right|^2}. \tag{6}$$

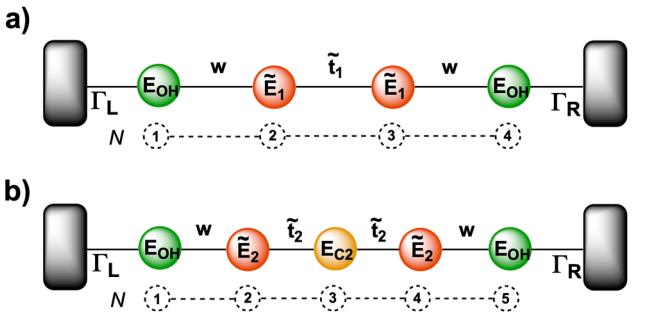

Fig. 4 Effective models for (a) hydroquinone, and (b) resorcinol. The colors of the atomic sites within each molecule correspond to an atomic site characterized by an effective Green's function or energy.

© 2025 The Author(s). Published by the Royal Society of Chemistry

Open Access Article. Published on 12 November 2025. Downloaded on 5/4/2026 11:46:22 PM. This article is licensed under a Creative Commons Attribution-NonCommercial 3.0 Unported Licence.

Here, the Green's functions G^0_{1N} and G^0_{NN} are analytically determined for each molecule. Specifically, we obtained for hydroquinone G_{14} and G_{44}, and for resorcinol G_{15} and G_{55}. These functions represent elements of the retarded Green's function matrix. Thus, the equations for the transmission probability for the hydroquinone (eqn (7)) and resorcinol (eqn (8)) are shown as follows:

$$T(E) = \frac{\Gamma^2 (G_{14})^2}{\left| \left[1 + \frac{i}{2}\Gamma G_{44}\right]^2 + \frac{\Gamma^2}{4}(G_{14})^2 \right|^2}. \quad (7)$$

$$T(E) = \frac{\Gamma^2 (G_{15})^2}{\left| \left[1 + \frac{i}{2}\Gamma G_{55}\right]^2 + \frac{\Gamma^2}{4}(G_{15})^2 \right|^2}. \quad (8)$$

We present the results of the decimation process for each molecule separately, following the geometric representation of Fig. 3. For further details on the mathematical procedure, see SI.

2.3 Current and conductance calculation

We used the Landauer–Büttiker formalism to calculate the electrical current values, establishing a relation between the material's electrical resistance and the scattering properties of electrons. This approach determines the electrical current flow in small electronic devices by accounting for quantum effects in electron transport. Thus, electrons propagate through the material while undergoing scattering at specific points. Consequently, the Landauer formula explains how these scattering events influence the material's electrical resistance and its ability to conduct current.[3,31,40,41]

Hence, an electron scattered through the molecule represents the current between the leads in aromatic molecules connected to electrodes. Applying the Landauer–Büttiker formalism, the current is given by the following equation:[3,13,18,29]

$$I(V) = I_0 \int_{-\infty}^{\infty} (f_L - f_R) T(E) \mathrm{d}E \quad (9)$$

where $I_0 = \frac{2e}{h}$, $T(E)$ is the transmission probability that an electron with an injection energy E reaches the output electrodes, and $f_{L(R)}$ is the Fermi–Dirac distribution, given by the following equation:[13,18,29]

$$f_{L(R)} = \frac{1}{1 + \exp\left(\frac{\varepsilon - \mu_{L(R)}}{k_B \Theta}\right)}. \quad (10)$$

Here, the chemical potential is given by $\mu_{L(R)} = \varepsilon_F \pm \frac{eV}{2}$, ε_F represents the Fermi energy, k_B is the Boltzmann constant, and Θ is the equilibrium temperature.[3,13,18,29,43]

By using the Landauer integral (ι_n) given by:

$$\iota_n = -\int T(E)(E - E_F)^n \left(\frac{\partial f(E)}{\partial E}\right) \mathrm{d}E \quad (11)$$

we calculate the electrical conductance (ς, with $n = 0$) by the following relation:[3,13,18,29,32–36,43]

$$\varsigma = \frac{2e^2}{h} \iota_0. \quad (12)$$

3 Results

3.1 Transmission probability

After applying the decimation process to resorcinol and hydroquinone, we evaluated the transmission probability (eqn (7) and (8)), along with a numerical analysis of quantum transport through these molecules. We considered two possible molecule–electrode coupling scenarios (Γ): weak and strong coupling, based on the relationship between electronic transmission probability within the molecule and the degree of hybridization.[3,13,18,29,43] Furthermore, several fundamental principles govern charge transport in single-molecule junctions, such as energy alignment and orbital broadening, which are closely related to hybridization (see SI).[11] Therefore, we cover the calculations at different coupling regimes to provide a more comprehensive understanding of the system's behavior. Thus, we determined the transmission probability ($T(E)$) in resorcinol and hydroquinone as a function of the incident electron energy

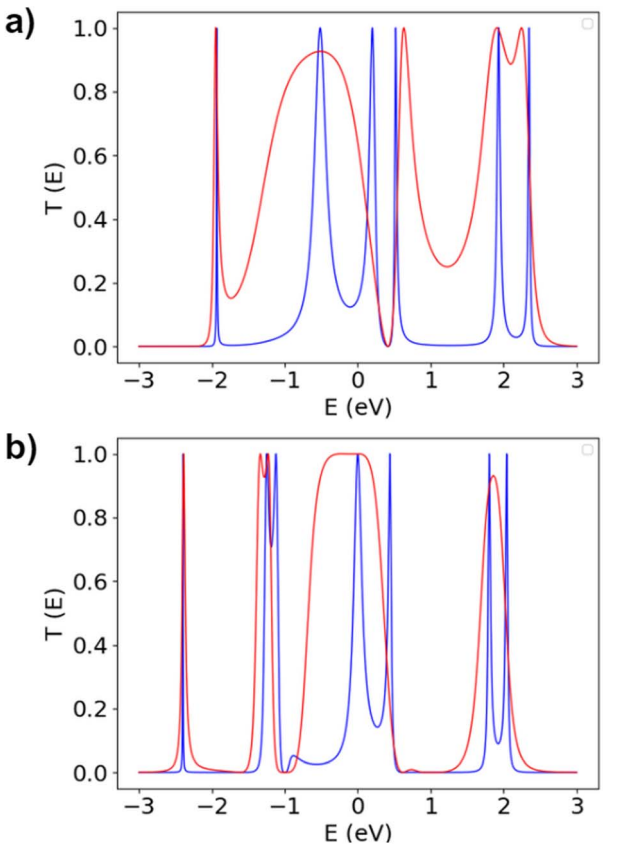

Fig. 5 Transmission probability under weak (blue) and strong (red) molecule–electrode coupling regimes for (a) hydroquinone and (b) resorcinol.

Open Access Article. Published on 12 November 2025. Downloaded on 5/4/2026 11:46:22 PM. This article is licensed under a Creative Commons Attribution-NonCommercial 3.0 Unported Licence.

(Fig. 5) varying the coupling. Specifically, we defined the parameters: $\Gamma = 0.2$ eV for the weak coupling regime (*i.e.*, $\Gamma < t$, w, blue line), $\Gamma = 2$ eV for the strong coupling regime (*i.e.*, $\Gamma > t$, w, red line), $E_1 = E_2 = 0.0$ eV, $E_{OH} = 0.0$ eV, $t = 1.0$ eV, $w = 1.0$ eV.

Observing the results of the $T(E)$ under a strong coupling regime, we distinguish a significant interaction between the aromatic molecule and the adjacent electrodes. This interaction might happen *via* hybridization between the molecular states and the continuum states of the contacts, leading to strong coupling, as evidenced by the broadening of the molecular states and suppression of some resonances in transmission compared to the weak coupling regime. For hydroquinone (Fig. 5a), this phenomenon becomes evident in two distinct energy ranges: from −2 eV to 0.4 eV and from 0.4 eV to 2.5 eV. Meanwhile, for resorcinol (Fig. 5b), this behavior is observed across three energy intervals: from −1.5 eV to −1 eV, from −1 eV to 0.5 eV, and 1.5 eV to 2.5 eV, approximately.

Fig. 5 presents a series of weak coupling regime resonant peaks correlating with the eigenvalues associated with the analyzed molecules. In the case of hydroquinone, those values are at −2.17 eV, −1.48 eV, −1 eV, −0.31 eV, 0.31 eV, 1 eV, 1.48 eV, and 2.17 eV, while for resorcinol, the eigenvalues are at −2.17 eV, −1.41 eV, −1.13 eV, -2.92×10^{-16} eV, -1.47×10^{-17} eV, 1.13 eV, 1.41 eV, and 2.17 eV. This correlation validates the decimation process applied in both systems, suggesting a strong influence of the molecular eigenstates on the electronic transmission dynamics in this coupling regime.

Interestingly, the quantum interference (QI) phenomenon is observable through the antiresonance peaks characterized by the eigenvalues of both molecules. These antiresonances represent the energy states where the transmission probability diminishes its value through the system.[13,18,29,48] This effect arises from the destructive interference between electron waves propagating through molecular orbitals in a single-molecule junction, leading to the appearance of distinctive energy peaks in the transmission probability curves. From a chemical perspective, we can visualize the phenomenon of QI more figuratively. In specific molecules, QI arises due to nodes in the molecular orbitals correlated with the chemical reactivity of the molecules. When the molecular orbitals generate nodes due to destructive interference, it leads to a preference for the localization of electrons in the chemical backbone.[11,48,49]

As an example, the reaction known as electrophilic aromatic substitution acts by the high electron density on the atoms, particularly those in the presence of activating groups (*ortho–para* directors). In such cases, electron-donating substituents typically avoid reacting at the *meta* position of the benzene ring due to the presence of a node, relative to the activating group, at the Highest Occupied Molecular Orbital (HOMO) of the molecular system.

From another perspective, Feynman's path integral theory in quantum mechanics exemplifies a node at the *meta* position; with an electron moving between two points, in this case the leads, it can explore all possible pathways simultaneously. The probability of finding the electron at a specific point is determined by the complex sum of all these possible trajectories. Thus, when a benzene ring links to two electrodes in a *meta* fashion, the Broglie wave vector of an electron at the Fermi energy level is defined by the equation $k_F = \pi/2d$, where d denotes the spacing between the carbon atoms in the benzene ring, which is 1.397 Å.[50] The direct pathways through the ring introduce a phase difference, leading to destructive interference and a notably low likelihood of electron transmission at this energy level. As a result, the paths through the benzene ring cancel out in pairs, creating a node in the transmission probability at the Fermi level. Specifically, the direct paths through the benzene ring have lengths of $2d$ and $4d$ (Fig. 6).These paths exhibit a phase difference that causes destructive interference. The accumulated phases of both paths enables us to determine their phase difference as follows:

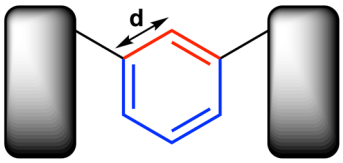

Fig. 6 Benzene linked in a *meta* fashion to two electrodes, depicting both path lengths 2d (red) and 4d (blue).

•Path = 2d

$$k_F \times 2d = \frac{\pi}{2d} \times 2d = \pi, \tag{13}$$

•Path = 4d

$$k_F \times 4d = \frac{\pi}{2d} \times 4d = 2\pi. \tag{14}$$

Thus, destructive interference results from the π phase difference. Hence, the transmission probability decreases at the Fermi energy level by having these electron trajectories, resulting in a node that hinders the electron coupling at this substituent's configuration, leading to the low conductivity of resorcinol (see *infra*). However, it is worth noting that quantum interference in a molecule does not necessarily imply a complete absence of conductivity. For instance, the waves cancel each other out in destructive interference, potentially reducing conductivity.[48,51]

In constructive interference, the waves can reinforce each other, allowing conductivity to be maintained or even increased more figuratively; resorcinol demonstrates quantum interference due to its resonance structures, unlike hydroquinone (Fig. 7). Since conductance quantifies the ability of electrons to flow between electrodes through a molecule, resorcinol clearly shows a lower conductance than hydroquinone by the QI phenomenon. Hydroquinone shows a direct electron movement through the aromatic ring, thus facilitating the electronic flux. The charges represented on the M atoms in resonance structures without QI indicate the charge transfer between electrodes, symbolizing efficiency in electrical conductivity. This striking difference in the conduction behavior between hydroquinone and resorcinol focuses attention on larger π-conjugated systems with specific substitution patterns, such as those

© 2025 The Author(s). Published by the Royal Society of Chemistry

Open Access Article. Published on 12 November 2025. Downloaded on 5/4/2026 11:46:22 PM. This article is licensed under a Creative Commons Attribution-NonCommercial 3.0 Unported Licence.

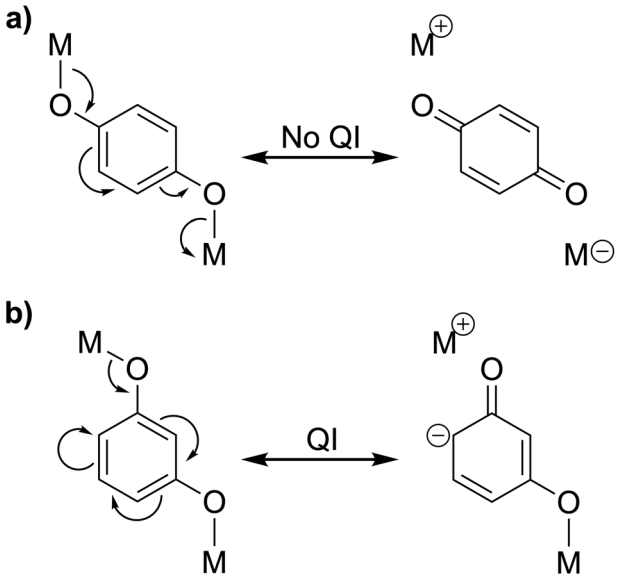

Fig. 7 Resonance structures of (a) hydroquinone and (b) resorcinol displaying where the quantum interference phenomenon (QI) occurs. M denotes any metal.

found in natural dyes.[17] Depending on the application, one might look for these systems. For instance, *para*-disubstitution might lead to a more efficient system for electronic transport,

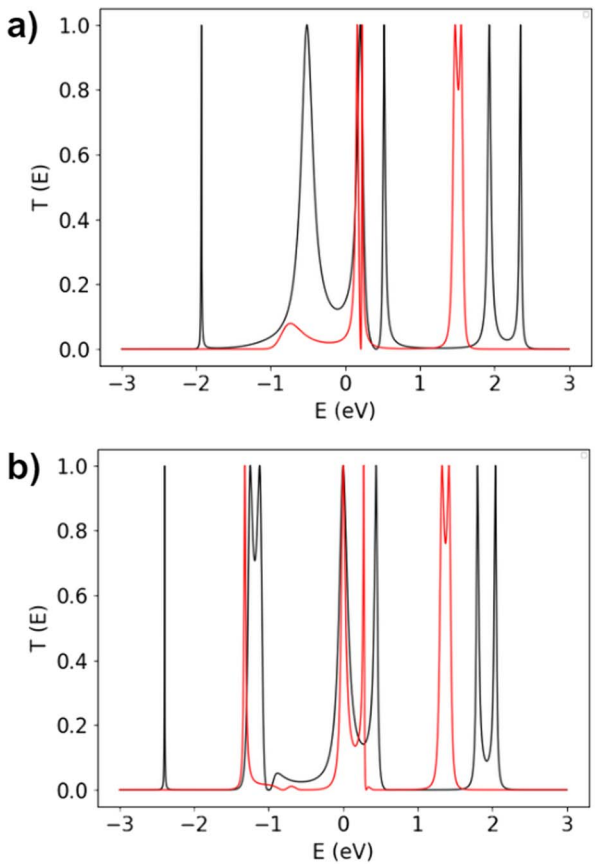

Fig. 8 Comparison of the transmission probability at weak coupling regime with $t = 1$ (black), and $t = 0.5$ (red) for (a) hydroquinone and (b) resorcinol.

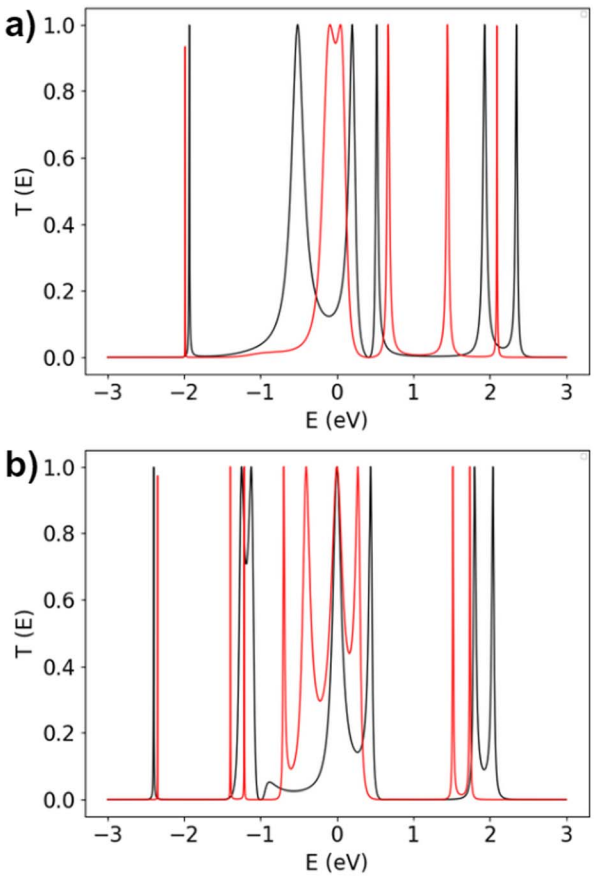

Fig. 9 Comparison of the transmission probability at weak coupling regime with $w = 1$ (black), and $w = 0.5$ (red) for (a) hydroquinone and (b) resorcinol.

whereas *meta*-disubstitution might be suitable for systems involving stepwise electron conduction.

We evaluated the influence of the internal couplings t and w on the electrical transport through the molecules in Fig. 8 and 9, respectively. Specifically, Fig. 8a and 9a correspond to hydroquinone, while Fig. 8b and 9b correspond to resorcinol.

To validate our analysis of transmission probability, we explored the weak coupling regime by varying the coupling parameters t and w. We found that the internal coupling within the aromatic ring (t) has a greater impact than the coupling between the hydroxyl group and the aromatic ring (w). This observation aligns with the principles of molecular hybridization. Within the benzene ring, each of the six carbon atoms adopts sp^2 hybridization, forming three sp^2 hybrid orbitals and one unhybridized p orbital perpendicular to these hybrids. These six p orbitals overlap laterally, creating a delocalized π-bonding system. Conversely, the oxygen atom in the hydroxyl group exhibits sp^3 hybridization. Two of its hybrid orbitals form sigma (σ) bonds with the hydrogen and carbon atoms, while the remaining two orbitals contain a lone pair of non-bonding electrons.

The delocalization of π electrons in the benzene ring favors electrical conductivity and thus has a more significant effect on electron transport than the σ bond in the hydroxyl group. This

© 2025 The Author(s). Published by the Royal Society of Chemistry

Open Access Article. Published on 12 November 2025. Downloaded on 5/4/2026 11:46:22 PM.
This article is licensed under a Creative Commons Attribution-NonCommercial 3.0 Unported Licence.

characteristic facilitates greater electron mobility along the conjugated system present in the aromatic ring. Some resonant peaks are suppressed in both molecules while the t coupling is varied. However, the effect is more pronounced in hydroquinone, thus illustrating that this coupling is directly involved in the accessible electronic states for electron transport through the molecules. The difference in symmetry in both molecules relates to the effect shown in the molecules.

The transmission probability changes significantly for resorcinol by lowering the coupling energy between the hydroxyl group and the aromatic ring (w). It represents a weakening of the interaction through the σ O–C bond, leading to more resonance peaks in the transmission probability. Under this coupling, the polarization effects of the electron density diminish from the hydroxyl group to the aromatic ring. In other words, decreasing the coupling energy lowers the interaction between the electrons of the hydroxyl group and those of the aromatic ring, allowing for a more discrete energy state.

To refine our model, we adjusted the atomic site energies to better represent the intrinsic properties of the atoms within the molecules. Specifically, we assigned a lower site energy to the hydroxyl groups compared to other atomic sites, considering factors such as electronegativity, hybridization, and interatomic interactions that shape the electronic environment of the

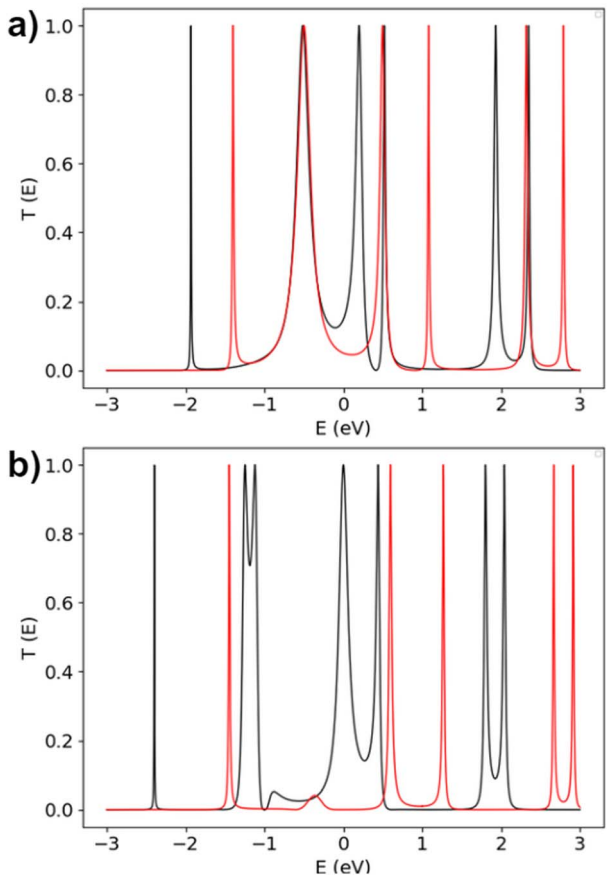

Fig. 10 Comparison of the transmission probability at weak coupling regime with $E_C = 0.0$ eV (black), and $E_C = 0.5$ eV (red) for (a) hydroquinone and (b) resorcinol.

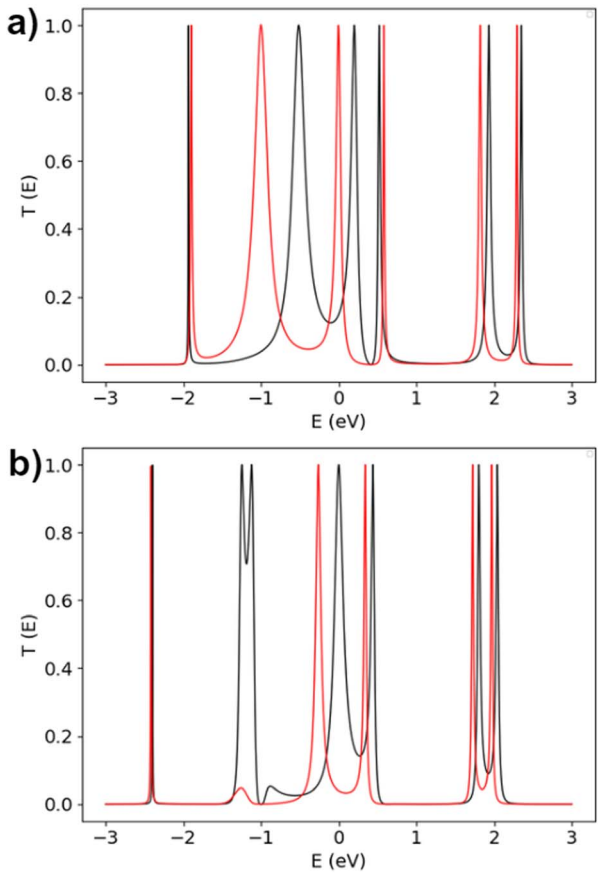

Fig. 11 Comparison of the transmission probability with $E_{OH} = 0.0$ eV (black) and $E_{OH} = -0.5$ eV (red) for (a) hydroquinone and (b) resorcinol.

hydroxyl group. We systematically varied the site energies of the carbon atoms ($E_{(C)}$) to 0.5 eV (Fig. 10) and the hydroxyl group ($E_{(OH)}$) to −0.5 eV (Fig. 11). As shown in Fig. 11, modifying $E_{(OH)}$ resulted in a slight leftward shift of the bands, indicating a reduction in the energy threshold required for electron transmission through the molecule. In contrast, adjusting $E_{(C)}$ (Fig. 10) caused a slight rightward shift of the bands, suggesting that a higher energy is needed to initiate electron transmission.

3.2 Current

After analyzing the transmission probability, we were intrigued by how the current in resorcinol and hydroquinone occurs. Interestingly, we observed a direct correlation between the normalized current (*i.e.*, I/I_0) and the applied voltage (Fig. 12) under both coupling regimes ($\Gamma < t$, w and $\Gamma > t$, w). The steps in the current relate to the voltage reaching a molecule's intrinsic value, producing a jump in the electron injection energy. We noticed that the molecular systems, either resorcinol or hydroquinone, under both coupling regimes, possess a typical semiconductor behavior. Additionally, when molecules reach their maximum electron storage capacity (*i.e.*, saturation), the stabilization of the current occurs, as evidenced by a plateau of the current. Even with a difference in the electrochemical potential, this passivation starts at nearly 5 Volts for hydroquinone and resorcinol, where the current amplitude is the highest.

© 2025 The Author(s). Published by the Royal Society of Chemistry

Open Access Article. Published on 12 November 2025. Downloaded on 5/4/2026 11:46:22 PM.
This article is licensed under a Creative Commons Attribution-NonCommercial 3.0 Unported Licence.

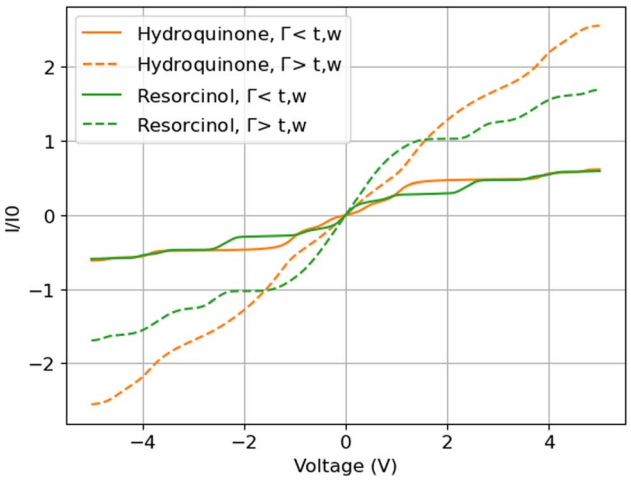

Fig. 12 Current *vs.* voltage for hydroquinone (orange) and resorcinol (green) at $\Theta = 300$ K, evaluated under weak (solid) and strong (dashed) coupling regimes.

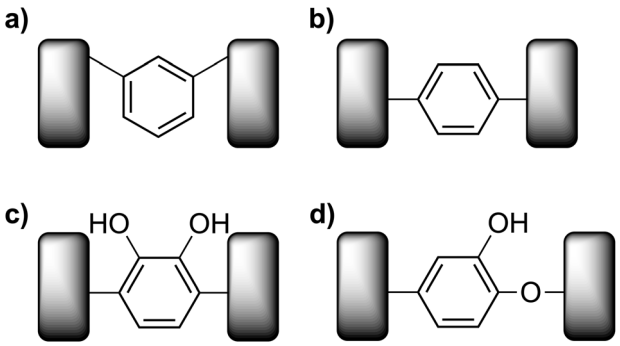

Fig. 13 Models used to calculate the electronic properties in benzene (a: Model I; b: Model II), and catechol (c: Model I; d: Model II). Adapted with permission from Ojeda *et al.* (2013).[13] Copyright 2013 AIP Publishing. Adapted from Soto *et al.* (2023).[18] Available under a CC-BY 4.0 license. Copyright The Authors.

Comparing the current values with similar systems studied previously, such as benzene and catechol linked in *meta* and *para* configurations (Fig. 13a and b for benzene, and Fig. 13c and d for catechol), the current conduction significantly varies among these molecules (Fig. 14) due to their structural and electronic differences.[13,18] In addition, the conduction capacity also depends on the link configuration of the molecule to the electrodes and whether QI phenomena are present.

Fig. 14 shows that benzene in a *para*-linked fashion (Model 2 Benzene) exhibits the highest current conduction capability of all evaluated systems. This good conductivity is attributed mainly to the symmetry of the linkage to the electrodes, facilitating an efficient electron flow. In contrast, the *meta*-linked benzene displays a destructive QI in its molecular structure, considerably reducing the conductivity capacity of this system (Model 1 benzene). Although hydroquinone presented the *para*-linked fashion to the electrodes, it shows lower conductivity than benzene in this configuration. This behavior is associated

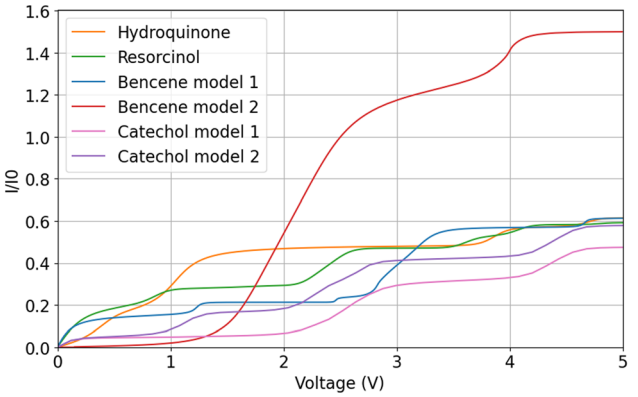

Fig. 14 Current *vs.* voltage for benzene-derived aromatic systems at $\theta = 300$ K, under a weak coupling regime. Data adapted with permission from Ojeda *et al.* (2013).[13] Copyright 2013 AIP Publishing. Adapted from Soto *et al.* (2023).[18] Available under a CC-BY 4.0 license. Copyright The Authors.

with the electronegativity of the elements comprising the molecular system, where the oxygen in the hydroxyl groups is more electronegative than hydrogen and carbon atoms, inducing molecular polarization through charge distribution differences. Thus, electrons tend to accumulate around the oxygen, leading to reduced current flow. However, hydroquinone is more conductive than the other benzenediol isomers (*i.e.*, catechol and resorcinol) due to the *para*-configuration of the hydroxyl substituents.

As shown in Fig. 12, resorcinol exhibits lower conductivity than hydroquinone. This difference is associated with the destructive QI phenomenon presented at resorcinol, with the appearance of a node in the molecular orbitals at the *meta* position, similar to *meta*-linked benzene. Interestingly, the evaluated models of catechol, in *para*-linked configurations to the electrodes, present the lowest conductivity of all systems. Specifically, due to the hydroxyl groups at the *ortho* positions at Model 1 of catechol, the electronic density polarization plays a crucial role in lowering the conductivity. In contrast, even though polarization is present, Model 2 of catechol presents higher conductivity than Model 1 because one of the hydroxyl groups favors polarization towards one of the electrodes in the direction of the electric flow.

In summary, polarization and the linkage configuration to the electrodes play a crucial role in the current passing through the molecule from one electrode to the other. Benzene exhibits the highest conductivity in *para*-linked fashion due to minimal polarization effects and the absence of destructive QI. Hydroquinone, despite polarization effects induced by hydroxyl groups, remains more conductive than resorcinol and catechol due to the favorable arrangement of its functional groups at the *para* position, reducing electronic density polarization effects.

Fig. 15 highlights a strong correlation between current, hydroquinone–electrode coupling, and applied voltage. As the coupling strength increases, the current becomes highly sensitive to voltage fluctuations, particularly in the positive voltage regime. This suggests that strong coupling enhances charge

Open Access Article. Published on 12 November 2025. Downloaded on 5/4/2026 11:46:22 PM.
This article is licensed under a Creative Commons Attribution-NonCommercial 3.0 Unported Licence.

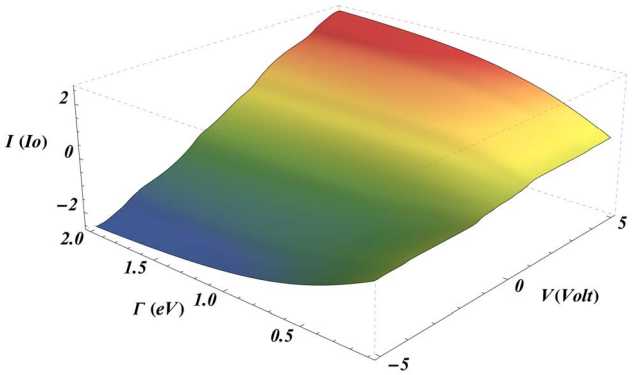

Fig. 15 Current as a function of hydroquinone–electrode coupling (Γ) and applied voltage (V).

transfer efficiency, making the system more responsive to external voltage biases. In contrast, weaker coupling results in a less pronounced current response, indicating reduced charge transport efficiency. This behavior stems from the alignment of molecular energy levels with the electrode Fermi level. Strong coupling improves this alignment, facilitating efficient electron tunneling between the molecule and electrodes. As a result, hydroquinone exhibits superior conductivity under strong coupling and high voltage conditions, making it a promising candidate for applications requiring dynamic current modulation.

Unlike hydroquinone, the resorcinol system (Fig. 16) exhibits a more gradual current response to changes in coupling strength and applied voltage. This suggests that its conductivity remains relatively stable across the range of evaluated parameters. The smoother current variation indicates that resorcinol is less likely to be altered by external factors, leading to a more consistent charge transport profile. Such stability is particularly beneficial in applications that require reliable performance despite voltage fluctuations. The behavior of resorcinol to sustain steady conductivity makes it well-suited for devices requiring stable charge transport, such as voltage regulators or precision control systems where maintaining a constant current flow is essential.

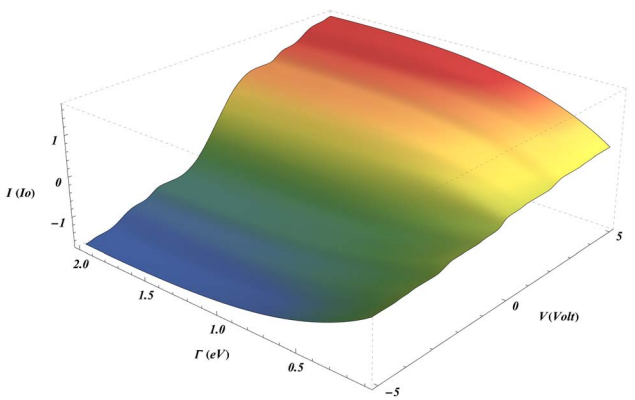

Fig. 16 Current as a function of resorcinol–electrode coupling (Γ) and applied voltage (V).

When comparing the 3D plots of both molecules for coupling values of 1.0 eV or higher, the hydroquinone demonstrates a remarkable ability to rapidly adjust its conductivity in response to small voltage variations. This characteristic is advantageous for electronic systems requiring dynamic conductivity tuning, such as molecular switches or sensors detecting subtle voltage shifts. Conversely, resorcinol maintains greater conductivity stability under the same conditions, making it ideal for applications where consistent performance is critical. In precision control systems, ensuring steady conductivity despite minor voltage changes is crucial for optimal functionality.

3.3. Conductance

Looking at the electrical conductance (Fig. 17), we observed an identical behavior to transmission probability, displaying the same number of resonant peaks at the same energy values. The local minima for hydroquinone and resorcinol represent two band gaps located around −2.2 eV:0.3 eV and −1.6 eV:1.0 eV, respectively. These peaks are associated with destructive QI between the molecule's localized states and the electrodes' delocalized states. The direct relation of the transmission probability to the conductance is trivial since both properties intrinsically relate to the ease with which the electrons pass through the molecules (*i.e.*, electrical current).

Fig. 17 provides a detailed overview of electron transport through the molecules, revealing significant differences in their electronic properties and electrode interaction. Resorcinol's conductance possesses pronounced conductance peaks around −2.4 eV, −1.3 eV, −1.1 eV, 0 eV, 0.4 eV, 1.8 eV, and 2.1 eV. The high density and narrow distribution of these peaks suggest the formation of multiple discrete energy levels that facilitate electron transport. Moreover, the peaks close to 0 eV indicate QI effects, where the molecule's energy levels strongly interact with the Fermi levels of the electrodes. In contrast, hydroquinone's conductance presents broader and fewer conductance peaks, observable around −1.9 eV, −0.5 eV, 0.1 eV, 0.5 eV, 1.9 eV, and

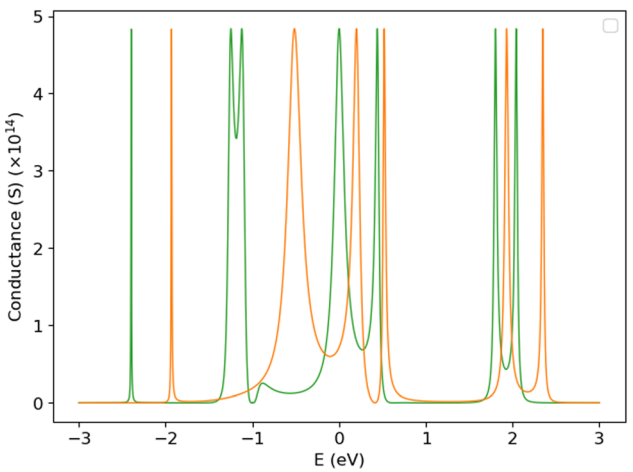

Fig. 17 Conductance *vs.* Fermi energy of resorcinol (green) and hydroquinone (orange) in a weak coupling regime.

© 2025 The Author(s). Published by the Royal Society of Chemistry

Open Access Article. Published on 12 November 2025. Downloaded on 5/4/2026 11:46:22 PM. This article is licensed under a Creative Commons Attribution-NonCommercial 3.0 Unported Licence.

2.3 eV. The broadening effect presented in the peaks for the hydroquinone proposes a strong coupling between the molecule and the electrodes, making electron transport more efficient at specific energy ranges. Like resorcinol, hydroquinone shows multiple peaks around 0 eV, indicating similar resonance effects.

4 Conclusions

In this study, we demonstrated that the system with resorcinol between the electrodes, characterized by a higher density of narrow peaks, offers multiple discrete channels for electron transport, enhancing conductance in systems operating across various energy levels. However, resorcinol (*i.e.*, *meta*-dihydroxybenzene) exhibits quantum interference (QI)/destructive interference leading to rapid fluctuations that may compromise its stability, thus reducing its conductance. In contrast, hydroquinone (*i.e.*, *para*-dihydroxybenzene) exhibits constructive interference, along with broader and fewer peaks, indicating stronger coupling with the electrodes, thus promoting more stable electron transport and efficient current flow. These observations are consistent with both theoretical and experimental literature. Indeed, Guédon *et al.* experimentally demonstrated destructive interference in charge transport through *meta*-connected molecules.[52] Pan *et al.* explored molecular conductance orbitals to understand interference patterns in aromatic frameworks,[53] while Chen *et al.* showed that quantum interference could enhance the performance of single-molecule transistors.[54] While the lower density and broader distribution of peaks in hydroquinone may limit conductance at certain energy levels, it contributes to a more stable and predictable electron transport behavior. Consequently, the selection between resorcinol and hydroquinone depends on the specific requirements of the molecular electronic application. Resorcinol fits in applications demanding higher conductance across multiple energy levels, whereas hydroquinone is preferable for scenarios where stability and efficiency at defined energy ranges are paramount.

Overall, we offered a novel perspective to study the electronic transport and the ring-electrode coupling effects by combining real-space decimation techniques with the investigation of the QI phenomena in structurally distinct molecules: resorcinol and hydroquinone. We showed that the coupling strength (Γ) plays a crucial role in modulating the position and sharpness of transmission resonances and influencing conductance behavior. This result is in agreement with recent studies that emphasize the impact of energy level alignment, orbital broadening, and anchoring group chemistry on hybridization and charge transport in molecular junctions,[11,55] as well as the effect of electrode materials and interface properties in modulating QI.[56,57] The decimation method allowed us to reduce system complexity while preserving essential topological features, making it particularly effective for small conjugated molecules where subtle structural differences can lead to significant variations in transport behavior. Our analysis provides a valuable foundation for the rational selection of molecular materials in the design of advanced electronic devices, emphasizing the importance of understanding and controlling conductance properties at the molecular level.

Author contributions

J. S. Martinez contributed to the data curation, formal analysis, visualisation and writing the original draft. D. Gallego contributed to the conceptualization of the project, formal analysis, project administration, writing original draft, review and editing. J. H. Ojeda contributed to the conceptualization of the project, formal analysis, project administration, writing original draft, review and editing.

Conflicts of interest

There are no conflicts to declare.

Data availability

Herein, on behalf of the authors, I declare that our manuscript entitled "Theoretical Determination of Electronic Properties of Resorcinol and Hydroquinone as Building Blocks of Molecular Wires", together with the supplementary information (SI) file, contains in detail the mathematical and calculation procedures to obtain the data we present within the results. We, the authors, are also open to receiving requests about data sharing with people interested in the results by the corresponding authors' email. Supplementary information is available. See DOI: **https://doi.org/10.1039/d5ra06041a**.

Acknowledgements

The authors thank to Universidad Pedagógica y Tecnológica de Colombia for providing the working space and resources necessary for the successful completion of this research.

References

1 H. Zhang, J. Li, C. Yang and X. Guo, *Acc. Mater. Res.*, 2024, **5**, 971–986.
2 R. T. Ayinla, M. Shiri, B. Song, M. Gangishetty and K. Wang, *Mater. Chem. Front.*, 2023, **7**, 3524–3542.
3 D. Xiang, X. Wang, C. Jia, T. Lee and X. Guo, *Chem. Rev.*, 2016, **116**, 4318–4440.
4 C. Toninelli, I. Gerhardt, A. S. Clark, A. Reserbat-Plantey, S. G"otzinger, Z. Ristanovi'c, M. Colautti, P. Lombardi, K. D. Major, I. Deperasi'nska, *et al.*, *Nat. Mater.*, 2021, **20**, 1615–1628.
5 X. Chang, Y. Huo, C. Zhao, W. Sun, Z. Song, Z. Qi, J. Wang, C. Jia and X. Guo, *Adv. Sensor Res.*, 2023, **2**, 2200084.
6 P. Wang, L.-Y. Zhang, A. Tzachor and W.-Q. Chen, *Nat. Comput. Sci.*, 2024, **4**, 818–823.
7 Y. Shao, M. Pala, H. Tang, B. Wang, J. Li, D. Esseni and J. A. del Alamo, *Nat. Electron.*, 2025, **8**, 157–167.
8 L. Chen, Z. Yang, Q. Lin, X. Li, J. Bai and W. Hong, *Langmuir*, 2024, **40**, 1988–2004.

Open Access Article. Published on 12 November 2025. Downloaded on 5/4/2026 11:46:22 PM. This article is licensed under a Creative Commons Attribution-NonCommercial 3.0 Unported Licence.

9 H. Fu, X. Zhu, P. Li, M. Li, L. Yang, C. Jia and X. Guo, *J. Mater. Chem. C*, 2022, **10**, 2375–2389.
10 E. Lörtscher, *Chem*, 2017, **3**, 376–377.
11 T. A. Su, M. Neupane, M. L. Steigerwald, L. Venkataraman and C. Nuckolls, *Nat. Rev. Mater.*, 2016, **1**, 16002.
12 C. A. Plazas Riaño, *PhD thesis*, Universidad Nacional de Colombia, 2011.
13 J. H. Ojeda, R. R. Rey-González and D. Laroze, *J. Appl. Phys.*, 2013, **114**, 213702.
14 N. Xin and X. Guo, *Chem*, 2017, **3**, 373–376.
15 X. Lv, C. Li, M.-M. Guo, W. Hong, L.-C. Chen, Q.-C. Zhang and Z.-N. Chen, *Molecules*, 2024, **29**, 2440.
16 S. P. Biswal, P. Hota, M. R. Dash and P. K. Misra, *Discov. Mol.*, 2024, **1**, 2.
17 S. Yadav, K. S. Tiwari, C. Gupta, M. K. Tiwari, A. Khan and S. P. Sonkar, *Results Chem.*, 2023, **5**, 100733.
18 E. Y. Soto-Gómez, J. H. Ojeda Silva, J. A. Gil-Corrales, D. Gallego, M. F. Hurtado Morales, A. L. Morales and C. A. Duque, *Condens. Matter*, 2023, **8**, 60.
19 R. M. Martin, *Electronic Structure: Basic Theory and Practical Methods*, 2nd edn, Cambridge university press, 2020.
20 J. Patterson and B. Bailey, *Solid-State Physics: Introduction to the Theory*, 2nd edn, Springer Berlin Heidelberg, 2010.
21 D. A. B. Miller, *Quantum Mechanics for Scientists and Engineers*, Cambridge University Press, 2008.
22 V. K. Jain, *Solid State Physics*, 3rd edn, Springer International Publishing, 2022.
23 C. Kittel and P. McEuen, *Introduction to Solid State Physics*, 8th edn, John Wiley & Sons, 2018.
24 E. Lazo, *Densidad de estados de sistemas de baja dimensionalidad*, Universidad de Tarapacá, 2001.
25 E. N. Economou, *Green's Functions in Quantum Physics*, Springer Science & Business Media, 2006, vol. 7.
26 K. Ohno, K. Esfarjani and Y. Kawazoe, *Computational Materials Science: from Ab Initio to Monte Carlo Methods*, 2nd edn, Springer, 2018.
27 K. Moth-Poulsen, *Handbook of Single-Molecule Electronics*, Jenny Stanford Publishing, 2016.
28 J. C. Cuevas and E. Scheer, *Molecular Electronics: an Introduction to Theory and Experiment*, World Scientific Publishing Company Pte Limited, 2010.
29 R. G. Toscano-Negrette, J. C. León-González, J. A. Vinasco, J. H. Ojeda Silva, A. L. Morales and C. A. Duque, *Condens. Matter*, 2023, **8**, 55.
30 V. Akimov, A. Tiutiunnyk, R. Demediuk, V. M. Tulupenko, E. Y. Soto Gómez, J. C. Cortés Peñaranda, P. A. Orellana Dinamarca, J. H. Ojeda Silva, J. A. Gil Corrales, J. C. León González and *et al.*, Study of delta-doped quantum wells, *Editorial Instituto Antioqueño de Investigación*, 2022.
31 J. H. Ojeda Silva, Una nanovisión electrónica de sistemas moleculares: aprendiendo acerca de transporte cuántico, *Editorial UPTC*, 2024.
32 H. M. Pastawski and E. A. M. Dagger, *arXiv: Mesoscale and Nanoscale Physics*, submitted on 9th Mar 2001, arXiv:cond–mat/0103219, accessed 2025-05-27.
33 P. S. Krstić, X.-G. Zhang and W. H. Butler, *Phys. Rev. B:Condens. Matter Mater. Phys.*, 2002, **66**, 205319.
34 K. Lambropoulos and C. Simserides, *Symmetry*, 2019, **11**, 968.
35 E. G. Emberly and G. Kirczenow, *Phys. Rev. B:Condens. Matter Mater. Phys.*, 1998, **58**, 10911–10920.
36 S. K. Maiti, *Chem. Phys.*, 2007, **331**, 254–260.
37 S. Datta, *Electronic Transport in Mesoscopic Systems*, Cambridge university press, 1997.
38 S. Datta, *Quantum Transport: Atom to Transistor*, Cambridge university press, 2005.
39 Y. V. Nazarov and Y. M. Blanter, *Quantum Transport: Introduction to Nanoscience*, Cambridge university press, 2009.
40 S. Forrest, *Organic Electronics: Foundations to Applications*, Oxford University Press, 2020.
41 M. Büttiker, Y. Imry, R. Landauer and S. Pinhas, *Phys. Rev. B:Condens. Matter Mater. Phys.*, 1985, **31**, 6207–6215.
42 W. Bro-Jørgensen and G. C. Solomon, *J. Phys. Chem. A*, 2023, **127**, 9003–9012.
43 J. H. Ojeda, L. Piracón-Muñoz, J. Guerra-Pinzón and J. A. Gómez-Castaño, *RSC Adv.*, 2020, **10**, 32127–32136.
44 Z. Zhouyin, X. Chen, P. Zhang, J. Wang and L. Wang, *Phys. Rev. B*, 2023, **108**, 195143.
45 A. Marie and P.-F. Loos, *J. Chem. Theory Comput.*, 2023, **19**, 3943–3957.
46 X. Lyu and N. Kawashima, *Phys. Rev. E*, 2025, **111**, 054140.
47 M. Ernzerhof, H. Bahmann, F. Goyer, M. Zhuang and P. Rocheleau, *J. Chem. Theory Comput.*, 2006, **2**, 1291–1297.
48 C. J. Lambert, *Chem. Soc. Rev.*, 2015, **44**, 875–888.
49 M. G. Reuter and T. Hansen, *J. Chem. Phys.*, 2014, **141**, 181103.
50 D. M. Cardamone, C. A. Stafford and S. Mazumdar, *Nano Lett.*, 2006, **6**, 2422–2426.
51 J. Liu, X. Huang, F. Wang and W. Hong, *Acc. Chem. Res.*, 2019, **52**, 151–160.
52 C. M. Guédon, H. Valkenier, T. Markussen, K. S. Thygesen, J. C. Hummelen and S. J. van der Molen, *Nature Nanotech.*, 2012, **7**, 305–309.
53 H. Pan, Y. Wang, J. Li, S. Li and S. Hou, *J. Phys. Chem. C*, 2022, **126**, 17424–17433.
54 Z. Chen, I. M. Grace, S. L. Woltering, L. Chen, A. Gee, J. Baugh, L. Briggs, G. Andrew and D. Bogani, J. A. Mol, C. J. Lambert and *et al.*, *arXiv: Mesoscale and Nanoscale Physics*, submitted on 17 Apr 2023, arXiv:2304.08535, accessed 2025–05–06.
55 A. Daaoub, J. M. F. Morris, V. A. Béland, P. Demay-Drouhard, S. J. Hussein, A. Higgins, H. Sadeghi, R. J. Nichols, A. Vezzoli, T. Baumgartner, *et al.*, *Angew. Chem., Int. Ed.*, 2023, **62**, e202302150.
56 A. Sarmah, P. Hobza, A. K. Chandra, S. Mitra and T. Nakajima, *ChemPhysChem*, 2024, **25**, e202300938.
57 O. Sengul, A. Valli and R. Stadler, *Nanoscale*, 2021, **13**, 17011–17021.

© 2025 The Author(s). Published by the Royal Society of Chemistry